1 # Self-assembled Star-shaped Chiroplasmonic Gold Nanoparticles

2 # for Ultrasensitive Chiro-immunosensor of Viruses

3 Syed Rahin Ahmed[1], Éva Nagy[2], and Suresh Neethirajan[1*]

4 [1]BioNano Laboratory, School of Engineering, University of Guelph, Guelph, Ontario,

5 Canada N1G 2W1

6 [2]Department of Pathobiology, Ontario Veterinary College, University of Guelph, Guelph, ON

7 N1G 2W1

8 [*]Corresponding author: sneethir@uoguelph.ca (SN)

9

10

11

12

13

14

15

16

17

18

19

1

20   Near field optics and optical tunneling light-matter interaction in the superstructure of chiral

21   nanostructures and semiconductor quantum dots exhibit strong optical rotation activity that

22   may open a new window for chiral-based bioanalytes detection. Herein we report an

23   ultrasensitive, chiro-immunosensor using superstructure of chiral gold nanohybrids (CAu

24   NPs) and quantum dots (QDs). Self-assembling techniques were employed to create

25   asymmetric plasmonic chiral nanostructures for extending the spectral range of circular

26   dichroism (CD) response for obtaining superior plasmonic resonant coupling with the QDs

27   excitonic state; this may help to achieve lower the limit of detection (LOD) values. As a

28   result, the designed probe exhibited avian influenza A (H5N1) viral concentration at

29   picomolar level, a significant improvement in sensitivity in comparison to a non-assembled

30   CAu NPs based chiroassay. The practicability of the proposed sensing system was

31   successfully demonstrated on several virus cultures including, avian influenza A (H4N6)

32   virus, fowl adenovirus and coronavirus in blood samples. The results of our study highlights

33   that exciton-plasmon interaction changes chirality and the self-assembled nanostructures are

34   an efficient strategy for enhancing the sensitivity of plasmonic nanosensors.

35

36

37

38

1. Introduction

Modern nanotechnology allows us to systematically manipulate the properties of nanoparticles by heterostructuring various nanomaterials either in one nanoscale structure or in alternating nanostructure surface morphologies, which serves as promising candidates for theoretical understanding, and in commercially viable technologies for biological applications. In particular, heterostructuring of semiconductor nanocrystal/plasmonic nanoparticles (PNPs) has garnered a lot of attention due to: (1) modified emission properties; (2) amplified absorption in the presence of plasmon resonance in the PNPs; and (3) shortening of exciton lifetime because of an increased radiation rate and energy transfer to the PNPs. The manipulation of the aforementioned properties of nanomaterials is vitally important and is considered a key issue for the development of technologies in the areas of nano-optics and nanoplasmonics.[1-6]

Recent years has seen a tremendous number of theoretical and experimental investigations of nanoplasmonics at near field optics with only few studies dealing with nano-chiroptics. The field of nano-chiroptics is a new emerging and an exciting frontier. The popularity of nano-chiroptics has exploded because of novel ways of fabrication of engineered metallic nanostructures with tunable surface morphology and their nano-assembly, which offers unprecedented control over electronic and optical properties[7].

58 Undoubtedly, light–matter interaction in chiral plasmonic metal-semiconductor nanohybrid

59 structures will introduce a new field in the sub-field of physical optics. The most significant

60 advantage of such nanohybrid structures is that they enhance chiroptical response, which

61 could be of great interest in a variety of applications related to chiral biosensing, opening up

62 new areas of research[8]. In comparison to natural chiral molecules, chiral plasmonic

63 nanostructures not only lead to large chiroptical effects, but they also introduce entirely new

64 concepts of superchiral light in technological applications.[9-11]

65

66 In the present study, we assumed that nano-assembly of CAu NPs and QDs through

67 immune-reaction could be used for bioanalytical purposes where chiro-optical properties

68 would be modified by a light-matter interaction. Previously, chiro-optical detection

69 techniques were developed based on assembling achiral plasmonic nanoparticles connected

70 by antigen-antibody bridges, and unexpectedly chirality was created due to either the homo-

71 plasmonic nanoparticles or the twisting of the hetero-plasmonic nanoparticles, thus achieving

72 exceptionally low LODs.[12-15] Several other methods of nano-assembling plasmonic

73 nanoparticles to generate circular dichroism based on DNA origami,[16,17] silica nanohelices as

74 chiral templates,[18] polymerase chain reaction,[19] DNA scaffolds[20] and specific non-covalent

75 interactions[21] have been reported. In addition, the broad understanding of plasmonic

76 structures for enhancing the chiroptical response has been studied both theoretically and

4

77   experimentally.[22] Herein, our approach is to enhance chiro-optical properties of CAu NPs by

78   nano-assembling with QDs through antibody-antigen interaction.

79   Nano-assemblies of chiral plasmonic nanoparticles with QDs may play a fundamental

80   role in an entirely new class of nanohybrids with optical resonances in both near field and far-

81   field coupling mechanisms and with enhanced chiroptical effects[7]. Plasmonic nanostructures

82   could play a vital role in achieving an excellent chiro-optical enhancement from metal

83   semiconductor nanohybrids as well as lower LODs for biosensing applications. Particularly,

84   plasmonic morphological alterations of nanostructure surfaces allows the tailoring of surface

85   Plasmon resonances and hence their interaction with incident light. Another important

86   component is the maximizing of overlapping absorption and emission spectra of CAu NPs

87   and QDs, respectively. Considering the above factors, we have developed a self-assembled

88   star-shaped chiro-plasmonic nanostructure using L(+)-ascorbic acid as a key material. We

89   have demonstrated the utility of this nanostructure by using it in a chiro-immunosensor of

90   avian influenza virus A (H5N1), targeting hemagglutinin (HA) and neuraminidase (NA)

91   surface proteins on virus.

92

93   We chose influenza virus A (H5N1) detection as a model analyte because of its high

94   pathogenicity in poultry and poultry consumers. The H5N1 flu strain is of great concern

95   globally due to high mortality rate, continuously expanding host range, and the potential

5

96   emergence of pandemic diseases. Highly pathogenic avian influenza viruses do not readily

97   transfer between humans; however, the disease can be transmitted from infected domestic

98   poultry to humans via close contact interactions (i.e., interaction with infected feces). The

99   effects of H5N1 can also be felt on a global economic level, as pandemic infections cause

100   large economic losses. Therefore, a rapid and sensitive detection tool for the identification of

101   influenza viruses are crucial for early detection and timely responses to overcome the

102   pandemic threat.[23-26]

103

104   In North America, fowl adenoviruses (FAdVs) are responsible for several diseases in

105   chickens namely hepatitis, hydropericardium syndrome, respiratory disease and

106   tenosynovitis, causing significant losses to the poultry industry worldwide every year. An

107   early detection system with high sensitivity and specificity is urgently needed to prevent the

108   spread out of disease in poultry sector.[27] Infectious bronchitis (IB), a coronavirus, is another

109   important disease of chickens caused by IB virus (IBV) which is one of the primary agents of

110   respiratory disease in chickens worldwide. Chickens susceptible to IBV infection have the

111   signs of gasping, coughing, rales, and nasal discharge, huddling together, appearing

112   depressed as well as wet droppings and increased water consumption.[28]

113   To demonstrate the real world applications of the proposed chiro-optical sensor, avian

114   influenza A (H4N6), fowl adenoviruses-9 (FAdVs-9) strain and infectious bronchitis virus

115   (IBV) were chosen as bioanalyte target candidates in this study.

2. Experimental Section

2.1 Materials and reagents

118   Gold (III) chloride trihydrate (HAuCl$_4$·3H$_2$O), cetyltrimethylammonium bromide (CTAB),

119   3,3',5,5'-tetramethylbenzidine (TMB), Hydrogen peroxide (H$_2$O$_2$), Poly-l-lysine (PLL), Nunc-

120   Immuno 96-well plates, CdTe QDs (emission wavelength 710 nm) were purchased from

121   Sigma-Aldrich (St. Louis, MO, USA). The anti-influenza A (H5N1) virus hemagglutinin

122   (HA) antibody [2B7] (ab135382, lot: GR100708-16), recombinant influenza virus A

123   (Avian/Vietnam/1203/04) (H5N1) (lot: GR301823-1), goat anti-mouse IgG, horseradish

124   peroxidase (HRP)-conjugated whole antibody (Ab 97023, lot: GR 250300-11) and

125   immunoassay blocking buffer (Ab 171534, lot: GR 223418-1) were purchased from Abcam,

126   Inc. (Cambridge, UK). Recombinant influenza virus A (H1N1) (California) (CLIHA014-2;

127   lot: 813PH1N1CA) was purchased from Cedarlane (Ontario, Canada). Influenza A (H5N2)

128   hemagglutinin antibodies (Anti-H3N2 antibodies HA MAb, Lot: HB05AP2609), Influenza A

129   (H7N9) hemagglutinin antibodies (Anti-H7N9 antibody HA MAb, Lot: HB05JA1903),

130   recombinant influenza virus A (H5N2) HA1 (A/Ostrich/South Africa/A/109/2006)(lot:

131   LC09AP1021),   recombinant   influenza   virus   A   (H7N8)   HA1

132   (A/Mallard/Netherlands/33/2006) (lot: LC09AP1323) and recombinant influenza virus A

133   (H7N9) HA1 (A/Shanghai/1/2013) (lot: LC09JA2702) were purchased from Sino Biological,

134   Inc. (Beijing, China). Avian influenza H5N1 neuraminidase polyclonal antibody (Cat. PA5-

135   34949)   was   received   from   Invitrogen   (Ontario,   Canada).   Anti-H4

136   (A/environment/Maryland/1101/06)(H4N6) polyclonal antibody was purchased from

137 MyBioSource Inc., San Diego, USA. Chicken whole blood (Cat. No: IR1-080N) was

138 received from Innovation Research, Michigan, USA. All experiments were performed using

139 highly pure deionized (DI) water (>18 MΩ·cm).

140

2.2 Preparation of different shaped CAu NPs

142 Chiral gold nanoparticles (CAu NPs) with different shapes were prepared by varying L(+)-

143 ascorbic acid concentrations. 20 µL of varying concentrations of L(+)-ascorbic acids (0.1,

144 0.05, 0.01, & 0.005 M) was mixed with 1 mL of 20 mM aqueous $HAuCl_4$ solution separately

145 under vigorous stirring at 25 °C. Color appeared within a few seconds based on L(+)-ascorbic

146 acids concentration indicating nanoparticle formation. Here, L(+)-ascorbic acids acts as both

147 the reducing agent and as a stabilizer as well as chiral ligands for CAu NPs.

148

2.3 Preparation of self-assembly chiral gold nanostructure

150 Self-assembled structures of CAu NPs were prepared as previously reported with slight

151 modifications.[12] For example, 10 mL of 2.5×10^{-4} M $HAuCl_4$ and 0.05 M CTAB were mixed

152 and gently stirred for 10 min. Then a 0.01 M (50 µL) solution of L(+)-ascorbic acid was

153 added to the mixture followed by the addition of 20 µL $AgNO_3$ (0.01 M) solution. Self-

154 assembled nanostructures were separated from solution by centrifugation at 2000 rpm for 10

155 min, and were redispersed in 1 mL water.

156

157   **2.4 Avian influenza A H4N6 virus culture**

158   Low pathogenic avian influenza virus A H4N6 (Avian influenza virus A/Duck/Czech/56

159   (H4N6)) was propagated in 11-day-old embryonated chicken eggs by inoculation into the

160   allantoic cavity.[29] Virus titer in allantoic fluid was determined at 72 h post-inoculation and

161   expressed as 50% tissue culture infective dose of 128 HAU/50 µL.

162

163   **2.5 Fowl adenoviruses-9 (FAdVs-9) virus culture**

164   FAdV-9 strain was propagated in chicken hepatoma cells (CH-SAH cell line) as described

165   previously.[30] CH-SAH cells were grown to confluency at 37°C, 5% CO_2 in Dulbecco's

166   modified Eagle's medium/nutrient mixture F-12 Ham with 10% non-heat-inactivated fetal

167   bovine serum as described previously. After infection with the virus, the cells were fed with

168   maintenance medium of D-MEM/F-12 with all the additions, except that the FBS was

169   reduced to 5%. FAdV-9 viral titer in allantoic fluid was determined as $5X10^7$ PFU/mL.

170

171   **2.6 Infectious bronchitis virus (IBV) culture**

172   The viruses were propagated and titrated as previously described.[31,32] The procedures were

173   carried out in specific pathogen free (SPF) embryonated eggs and the titers were determined

174   by the method of Reed and Muench.[33] The stock solution of viral titers was 1×10^6

175   EID_{50}/mL.

9

176

2.7 Specificity of antibodies towards target influenza A (H5N1) virus

178 Conventional ELISA method was performed to check the specificity of the anti-H5N1 HA

179 (Ab 135382) for influenza virus A/ Vietnam 1203/04/2009 (H3N2). A total of 50 µL

180 (1µg/mL) of virus solution in PBS buffer (pH 7.5) was added to PS plate and kept overnight

181 at 4°C. The next day, wells were rinsed three times with PBS buffer (pH 7.5), immunoassay

182 blocking buffer (Ab 171534, 100 µL) was added and kept at room temperature for 2h. After

183 rinsing three times with PBS buffer (pH 7.5) solution, anti-H5N1 HA Ab (1 µg/mL), anti-

184 H5N1 NA antibody (1 µg/ml), anti-H5N2 HA antibody (1 µg/ml), and anti-H7N9 HA

185 antibody (1 µg/ml) were added to each of the wells, and the plate was incubated at room

186 temperature for 1 h. Again it was washed with PBS buffer (pH 7.5), and HRP-labelled

187 secondary antibody (50 µL, 1 µg/mL) was added and incubated at room temperature for 1h.

188 Then unbound or loosely bound secondary antibodies were washed out using PBS buffer (pH

189 7.5), and TMBZ (10 nM)/H_2O_2 (5 nM) solution was added to each well (50 µL/well) for 10

190 min at room temperature. The enzymatic reactions were stopped by adding 10% H_2SO_4

191 solution (50 µL/well), and the absorbance of the solutions was recorded using a microplate

192 reader (Cytation 5, BioTek Instruments Inc., Ontario, Canada) at 450 nm.

193

2.8 Anti-H5N1 HA (Ab 135382) conjugation with self-assembled CAu nanostructures

195 Target virus-specific antibodies (anti-H5N1 HA Ab 135382) were bound to self-assembled

196   nanostructures of CAu NPs through electrostatic bonds. 1 mL of positively charged (+12.38

197   eV) CAu nanostructures were mixed with negatively charged (-2.31 eV) HA Ab 135382

198   antibody (1 µL, 5 ng/mL) and continuously stirred for 2h at room temperature. The mixture

199   was then centrifuged (4000 rpm for 10 min) and washed 3 times with PBS buffer to remove

200   the unbound components. To check the antibody-nanostructure binding, samples were

201   blocked with 2% BSA (100 µL) for 2 h at room temperature. After centrifugation and

202   washing steps, 1 ng/mL (50 µL) of anti-mouse IgG-horseradish peroxidase (HRP) (Santa

203   Cruz Biotechnology, CA) was added to each well followed by incubation at room

204   temperature for 1 h. Upon adding a total of 100 µL TMBZ substrate solution (10 µg/mL,

205   TMBZ, 10% H_2O_2 in 100 mM NaOAc, pH 6.0) to each well for 5–30 min at 25°C.

206   Enzymatic color developed (blue color) at this stage, and the reaction was stopped by adding

207   10% H_2SO_4 (100 µL), and absorbance was recorded at 450 nm with a reference at 655 nm.

208

2.9 Binding of anti-H5N1 NA with carboxyl capped QDs using ELISA

210   Carboxyl capped CdTe QDs were bound with antibodies through EDC/NHS chemistry. 1 mL

211   of QDs were placed in a 1.5 mL microfuge tube followed by adding 4 mM of EDC, NHS (10

212   mM) and 1 µL anti-NA antibodies (5 ng/mL), and the mixture was gently stirred at 10°C. To

213   confirm the binding between QDs and antibodies, ELISA was performed as follows:

214   Centrifuged (1000 rpm, 10 min) and washed to remove unbound antibodies or other reagents,

215   then the conjugated part was blocked with 2% BSA for 1h. Anti-mouse IgG-HRP (Santa

216   Cruz Biotechnol., CA) (50 µL, 1ng/mL) was then added in each well after washing steps and

217   then incubation for 1h at room temperature. Samples were washed after centrifugation three

218   times, and 50 µL TMBZ substrate solution (10 µg/mL, TMBZ, 10% H_2O_2 in 100 mM

219   NaOAc, pH 6.0) was added to each well and allowed to stand for 5–30 min at 25°C. At last,

220   the reaction was stopped by adding 50 µL of 10% H_2SO_4 and the absorbance was recorded at

11

221   450 nm.

222   **2.10 Chiro-optical detection of Influenza virus A (H5N1)**

223   Chiral based optical sensing experiments were performed after confirming the binding of

224   anti-H5N1 HA (Ab 135382) with CAu nanostructures and QDs using ELISA method.

225   100 µL of anti-HA Ab-conjugated CAu nanostructure containing varying concentrations of

226   recombinant influenza A (H5N1) in PBS buffer were added to the CD cuvette. Then, 100 µL

227   of anti-NA Ab-conjugated QDs were added, and the CD response was checked. Other

228   influenza viruses were examined in the same manner as a negative control. The samples were

229   excited at 380 nm, and the exciting and the emission slits were at 5 and 5 nm, respectively.

230   Based on the chiro-optical response at different concentrations of target virus, a statistical

231   curve was constructed. In case of clinical virus culture samples, influenza A (H4N6), 50 µL

232   of anti-HA Ab-conjugated CAu nanostructure containing varying concentrations of

233   recombinant influenza A (H4N6) in chicken blood samples were added to the CD cuvette.

234   Then, 100 µL of anti-NA Ab-conjugated QDs were added, and the CD response was

235   recorded. Similar sensing method was followed in case of fowl adenoviruses-9 (FAdVs-9)

236   strain and Infectious bronchitis virus (IBV) detection.

237

238   **2.11 Validation with commercial ELISA kit**

239   A comparison experiment was performed with the commercial avian influenza A H5N1

240   ELISA kit (Cat. No: MBS9324259, MyBioSource, Inc., San Diego, USA) to validate our

241   proposed method. Different concentrations of virus solution were prepared using sample

242   diluent that was received with the commercial ELISA kit strictly maintaining the

243   manufacturer's protocol during bioassay. Color developed with different absorbance intensity

244   related to viral concentration in the 96-well plates was recorded at 450 nm. Influenza A

245   (H4N6) virus detection was also validated with commercially available ELISA kit (Cat. No:

246   NS-E10156, Novatein Biosciences, Woburn, USA). The assay procedure was strictly

247   followed as mentioned in the protocol book.

248   **2.12 Spectroscopy and structural characterization**

249   Transmission electron microscopy (TEM) images were captured using Tecnai TEM (FEI

250   Tecnai G2 F20, Ontario, Canada). Zeta potential was measured with Zetasizer Nano ZS

251   (Malvern Instruments Ltd., Worcestershire, UK). Circular Dichroism spectrum was recorded

252   using JASCO CD Spectrometer (Model: J-815, Easton, USA).

253

254   **3. Results & Discussions**

255   Artificial chiral plasmonic nanomaterials demonstrate extraordinary rotational ability of

256   polarizing light by engineering intra-particle couplings with light-emitting nanomaterials at

257   nanoscale gap in comparison to naturally occurring chiral materials. This concept was

258   utilized in our study to develop chiro-immunosensor that employs exciton-plasmon

259   interaction in chiral gold nanoparticles (CAu NPs) – CdTe QDs nanohybrids. Two different

260   anti influenza virus surface protein antibodies named anti-HA and anti-NA were bound to

261   CAu NPs and QDs, respectively. Then, a nano-sandwich structure was formed with the

262   addition of target influenza virus A/ Vietnam 1203/04/2009 (H3N2). The amount of CAu

263   NPs and QDs taking part in the nano-assembling process totally depends on the viral

264   concentration. Hence, chiro-optical changes would be influenced by the CAu NPs-QDs

265   nanohybrids. With our proposed sensing concept, it is reasonable to move to a chiro-

266   plasmonic rough surface that has more light scattering properties as well as confined energy

267   in space and enables the creation of a strong coupling regime and increased optical non-

268   linearities through light-matter interactions with QDs.[1,34] Such strong localization of energy

269   in nanoscale gap may provide specific spatial positions to tune and further enhance the

270   chiral property of CAu NPs efficiently.

271

272   In order to fully exploit the nanostructured morphology, a series of differently shaped

273   (hetero-structured) CAu NPs were prepared by varying L(+) ascorbic acid concentration

274   during the reaction process. As shown in Figure **1**, different sizes and morphologies of CAu

275   NPs were obtained by using various concentrations of L(+) ascorbic acid in 20 mM $HAuCl_4$

276   solution. Prolate shaped CAu NPs were obtained with a diameter of 50 nm at 0.1 M L(+)

277   ascorbic acid (Fig. 1A). As the concentration of L(+) ascorbic acid shifted from 0.1 M to

278   0.005 M (Figure 1 A–D), the CAu NPs structure ranged from well-defined simple flower-like

279   (Fig. 1B), urchin (Figure 1C), and dendritic-type morphologies (Fig.1D). It should be noted

280   that urchin shaped CAu NPs with many spikes were obtained when the concentration of L(+)

281   ascorbic acid was 0.01M (Fig. 1C). Unfortunately, though dendritic-shaped CAu NPs

282   contained many arms and branches on their structural morphology, spectroscopic study

283   showed a very weak plasmonic peak (Fig.2). The plasmonic peaks obtained from prolate,

284   flower, and urchin shaped CAu NPs were located at 548 nm, 565 nm, and 590 nm,

285   respectively. Among them, urchin shaped CAu NPs was chosen for further experiments due

286   to the numerous spikes on their surface as well as a broadened plasmonic peak, which offers

287   the possibility of having maximum overlap, and coupling with the excitonic wavelength of

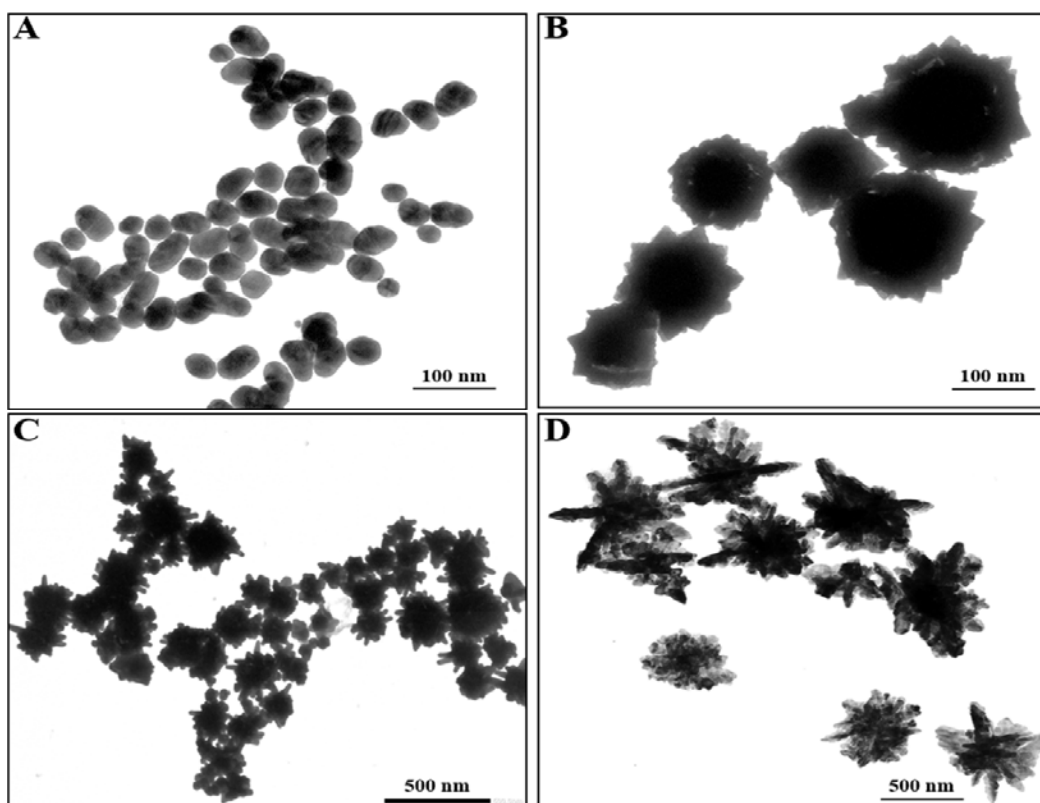288   QDs, which may strengthen the optical activity.

289

290

Figure 1: Transmission electron microscopic image of the developed CAu NPs; (A) Prolate-

like, (B) Flower-like, (C) Urchin-like & (D) Dendritic shaped CAu NPs.

293

294   Enhanced localized surface plasmon resonance (LSPR) could potentially serve as an effective

295   platform to prove that the hetero-structured nanoparticles have enough sensitivity for

296   bioanalytical detection.[35] With this concept in mind, the self-assembled structure of star-

297   shaped nanoparticles was prepared by the addition of CTAB that served as a 'glue' to link the

298   {100}facets of two adjacent CAu NPs, which in-turn aided in organizing the chiral gold

299   nanostructure into a short chain.[36] Star-shaped CAu nanostructures with varying morphology

300   is shown in Figure 4, with spike length and diameter of 10 nm and 2 nm, respectively (Fig.

16

301   3F).

302
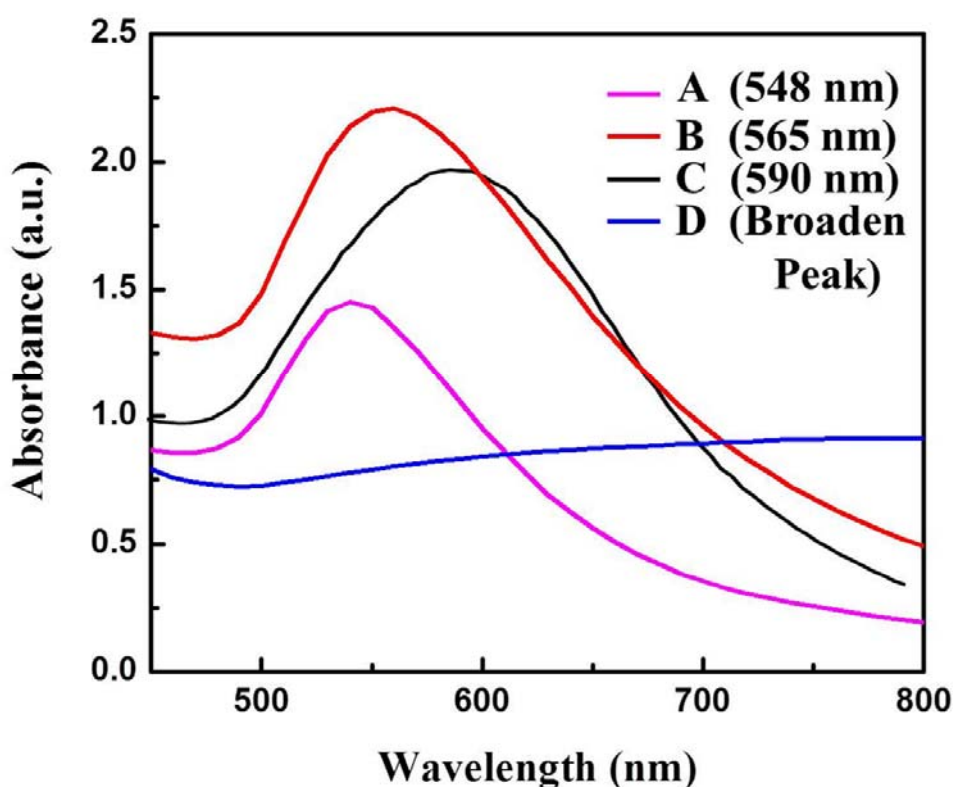
Figure 2: UV-visible spectra of different shaped CAu NPs; (A) Prolate-like, (B) Flower-like,

(C) Urchin-like & (D) Dendritic shaped CAu NPs.

305

306   CdTe NPs was chosen to make nanohybrids with CAu NPs due to its strong emission

307   properties and energy overlap possibility between the excitonic and plasmonic states of the

308   resulting nanohybrids. Photoluminescence spectra (PL) and ultra-violet (UV) spectra of QDs

309   are shown in Fig. S1A; the emission peak was located at 710 nm. Particle size and

310   concentration were 6.5 nm and 3.7×10^{-7} M, respectively, calculated based on Peng equation.[37]
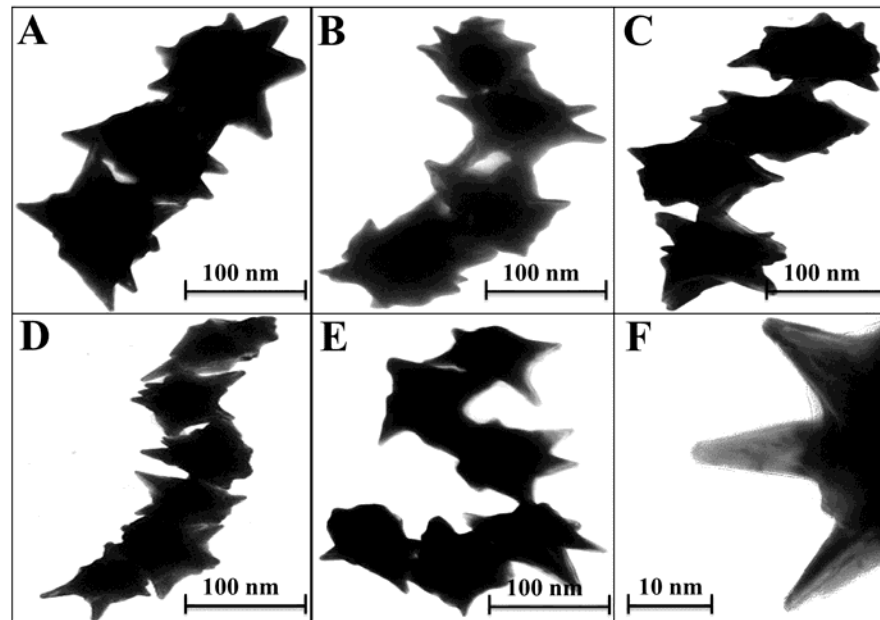
311

312

313

314 **Figure 3:** Transmission electron microscopic image of the self-assembled chiro-plasmonic

315 nanostructures; (A) short straight chain, (B) left turned chain, (C) right turned chain, (D) long

316 chain with short angled curve chain, (E) long chain with high angled curve chain & (F) close-

317 up image of spikes of CAu NPs.

318

319   The specificity of anti-influenza A (H5N1) virus hemagglutinin (HA) antibody Ab

320 135382 against recombinant influenza virus A (Avian/Vietnam/1203/04) (H5N1) was

321 confirmed using a conventional ELISA method. Figure S1B shows that the optical density

322 obtained due to enzymatic activity for the target virus/Ab 135382 HA/HRP-conjugated

323 secondary antibody/ TMBZ–H_2O_2 complex, and the target virus/anti-H5N1 NA/HRP-

324 conjugated secondary antibody/ TMBZ–H_2O_2 complex was higher than those of anti-H5N2

325 HA and anti-H7N9 HA Ab, implying the specificity of Ab 135382 towards recombinant

326 influenza virus A (Avian/Vietnam/1203/04) (H5N1). The higher optical density obtained for

327 anti-H5N1 Ab 135382 and CAu nanostructures complex in ELISA results confirmed the

328 successful binding between anti-H5N1 Ab 135382 and CAu nanostructures (Fig. S2A).

329
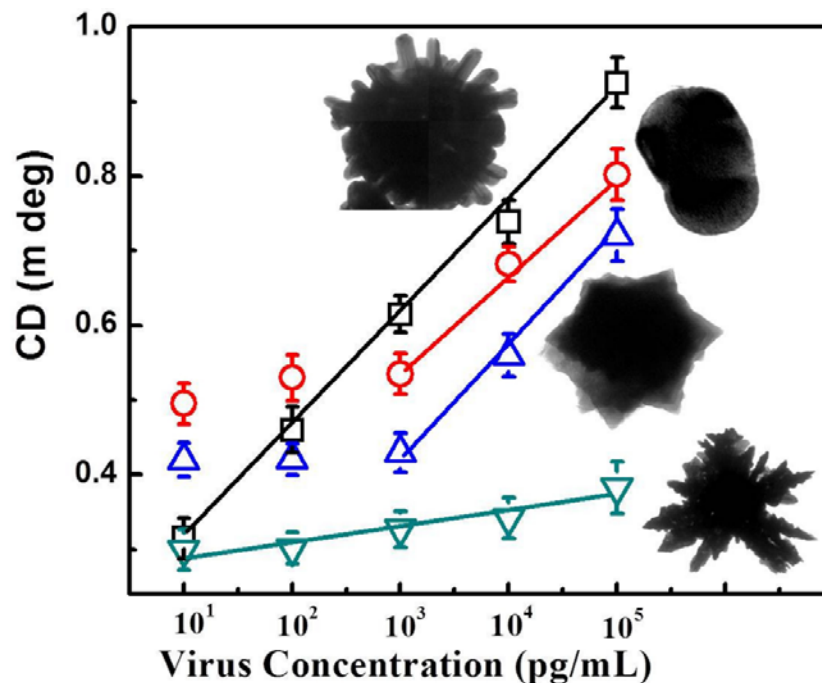
Figure 4: Comparison of the detection performance of different shaped CAu NPs; CD

331 spectrum Vs target virus sensing results.

332 The binding between anti-H5N1 Ab 135382 and CdTe QDs was confirmed by FTIR

333 spectrum. As shown in Fig. S2B, FTIR bands found at 3500–3700 cm^{-1} for amide N–H

334 stretching represents the chemical binding between Ab 135382 and CdTe QDs, whereas only

335 carboxylic acid O-H stretching bands appeared for CdTe QDs alone. The influence of the

19

336   structural morphology on the sensitivity of a chiro-sensor was further investigated to enable

337   the selection of the optimized shape of the CAu NPs for the bioassay platforms. Four typical

338   CAu NPs structures, prolate shaped CAu NPs, flower-shaped CAu NPs, spiky-like CAu NPs

339   and dendritic shaped CAu NPs were selected to construct nanohybrids with QDs through

340   immune-reaction for a chiral biosensor for avian influenza virus detection. It was found that

341   the optical response of the biosensors was largely dependent on the total amount of analytes

342   assembled on these CAu NPs. As shown in Figure 4, the linear detection ranges of CAu NPs

343   were drastically influenced by the nanostructure's shape. The detection range of urchin-like

344   CAu NPs was 10 pg to10 µg/mL, whereas for prolate and flower shaped CAu NPs, the range

345   was between 1 ng to 10 µg/mL.

346

347   Experimental results revealed that chiro-optical response from dendritic shaped CAu NPs

348   was not significant; probably due to a weak plasmonic peak. In general, rough nanostructures

349   have higher analytes capture efficiency in the bioassay applications than that of the smooth

350   nanostructures, and this ultimately influences the detection limit of a biosensor. Compared

351   with other CAu NPs, urchin shaped nanostructures possessed higher surface to volume ratio

352   as well as stronger plasmonic peak; therefore, we chose urchin shaped CAu NPs to construct

353   the self-assembled chiro-plasmonic nanostructures.

354

20

355   Nano-sandwich assembly was formed via the addition of various concentrations of

356   recombinant influenza virus A (H5N1) to antibody conjugated self-assembled CAu

357   nanostructure and QDs solutions. Chiro-optical response and plasmonic response of viral

358   concentration were carefully examined (Fig. 5A & 5B), and a calibration curve for chiro-

359   optical detection of avian influenza virus was constructed. The sensitivity of the bioassay was

360   found up to 1 pg/mL (Fig. 5C), 10 times more sensitive than the non-assembled urchin-like

361   CAu NPs. Most probably, multi-times scattering of incident light on the plasmonic rough

362   surface confined lots of energy in space, which ultimately influence the chirality of CAu

363   nanostructures. A plasmon-based bioassay was performed using the same standard viral

364   concentrations, but the plasmonic response did not significantly correlated with the viral

365   concentrations. In the case of conventional ELISA method, the sensitivity was found to be 1
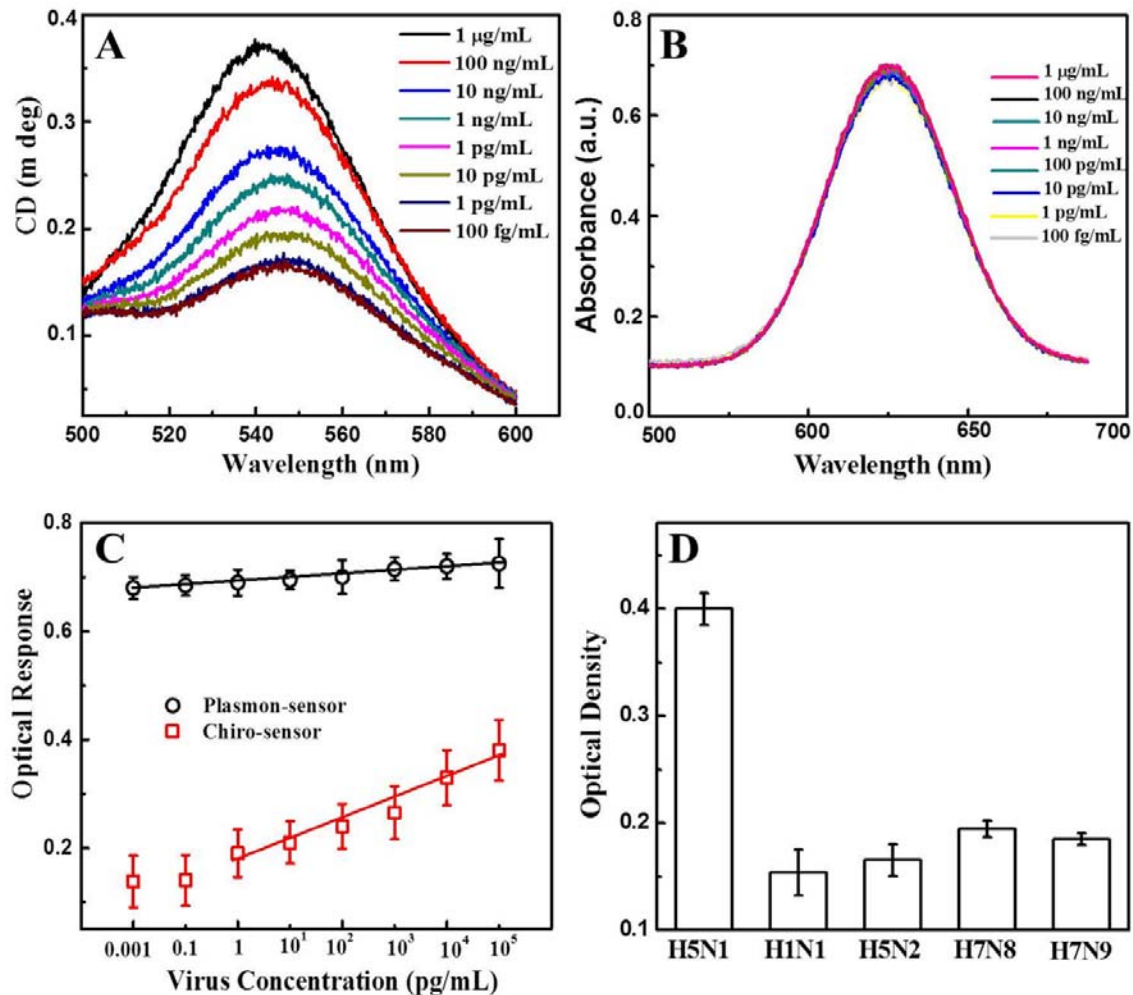
366   ng/mL level.

367

368

369

Figure 5: Detection of the avian influenza virus; (A) Chiro-optical spectra of different concentration virus detection, (B) Plasmonic spectra of different concentration virus detection, (C) Analytical calibration curves relating the intensity of circular dichroism (CD) and plasmonic spectra & (D) Selectivity of proposed bioassay.

The selectivity test of the proposed bioassay was implemented with other virus strains, namely H1N1, H5N2, H7N8 and H7N9; a significant chiro-optical response (8~9-fold

22

379   higher) was obtained with the target avian influenza virus A (H5N1) in comparison to the

380   others, revealing that the current bioassay is sufficiently selective for the detection of target

381   avian influenza virus A (H5N1) (Fig. 5D).The sensitivity of the developed chiro-optical

382   sensor was validated with the commercial colorimetric detection kit for avian influenza A

383   (H5N1) (Table 1 & Fig. S3). The visual color response of the commercial kit was up to 1

384   ng/mL, indicating that the chiro-optical response-based bioassay is more sensitive than the

385   commercial kit.

386

387   **Table 1:** Comparison of avian influenza virus A (Avian/Vietnam/1203/04) (H5N1)

388   detection using different methods

389

Detection method	Virus concentration (pg/mL)								
	10^7	10^6	10^5	10^4	10^3	10^2	10	1	0
This study	+	+	+	+	+	+	+	+	−
Conventional ELISA	+	+	+	+	+	−	−	−	−
Commercial kit	+	+	+	+	+	−	−	−	−

390

391

392   We also explored the practical application of the developed chirosensor in the PBS buffer

393   and in chicken blood samples for influenza A (H4N6) virus detection that represents a

394   complex biological mixture. The detection of the Avian influenza A (H4N6) virus

395   concentration is dependent on the amount of CAu nanostructures and QDs presents in nano-

396   assembled structure and hence is directly associated to the optical activity of the resulting

397   dispersions. Upon confirming the anti-H4N6 antibody specificity towards the real avian

398   influenza A (H4N6) virus (Fig. S4) and its binding confirmation with CAu nanostructure and

399   QDs (Fig. S5); a calibration curve for chiroplasmonic detection of influenza A (H4N6) virus

400   was obtained by the standard dilution method (Fig. 6A). The linear range of the influenza A

401   (H4N6) virus detection in PBS buffer was found to be from 100 to 0.01 HAU/50 µL with the

402   limit of detection 0.0268 HAU/50 µL. The proposed chirosensor exhibited its detection

403   ability at complex media with the linear range of 100 to 0.01 HAU/50 µL; the limit of

404   detection was 0.0315 HAU/50 µL calculated by standard deviation method. Here, bovine

405   serum albumin (BSA) and influenza virus A (H5N1) were used a control. The validated

406   ELISA results confirmed the superiority of the proposed technique in terms of sensitivity

407   over the commercial kit (Table S1). FAdVs-9 viruses in blood samples were detected

408   followed by confirming the successful binding of anti- FAdVs antibody through ELISA

409   method (Fig. S6). The sensitivity of the chiral response based bioassay for FAdVs-9 detection

410   showed up to 50 PFU/mL with the limit of detection of 33.64 PFU/mL (Fig. 6B) and the

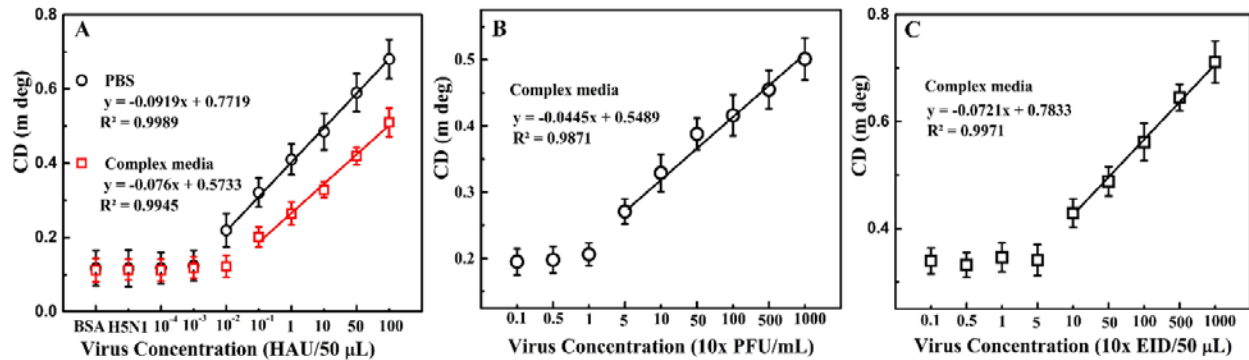411   assay confirmed the highly selectivity as well (Fig. S7).

24

412

413

Figure 6: Detection of the multiple virus culture samples; (A) avian influenza virus A (H4N6); Closed Circles (black) and square (red) represent the sensing results of A (H4N6) detection in PBS buffer and complex matrix (chicken blood) respectively, (B)   fowl adenovirus (FADV) and (C) Infectious bronchitis virus (IBV) detection in chicken blood media.

420

Our proposed bioassay system was further applied for infectious bronchitis virus (IBV) detection in blood samples after confirming successful binding of CAu nanostructures and QDS with IBV specific antibody (Fig. S8). The chiroptical response of IBV detection was observed to be in the range of $10^2 \sim 10^4$ EID/50 µL with the limit of detection of 47.91 EID/50 µL (Fig. 6C) and the assay confirmed selectivity for only the target analytes (S9).Thus, the proposed chiral-based biosensor enable the utilization of this technique in real life applications.

428

4. Conclusions

430   Chiral biosensors will be at the forefront of the bionanotechnology field in the near future due

431   to the ultra-sensitivity and rapid response time. Our work demonstrates a framework and a

432   method to achieve enhanced sensitivity using chiral metal nanoparticles–quantum dot

433   nanocomposites for detecting bioanalytes in clinical samples. While the proposed sensing

434   method was applied to the colloidal CAu NPs and self-assembled CAu nanostructure; the

435   latter showed better detection performance due to the multipole plasmonic scattering effects

436   on the rough CAu nanostructure. Sensitivity on the order of pico-gram level was achieved,

437   which is superior than the conventional ELISA methods, the plasmonic biosensor and the

438   commercial kits. The sensing performance of the proposed method was also retained in

439   complex biological media for avian influenza A (H4N6) virus, fowl adenovirus and

440   coronavirus. The simplicity and more importantly, the concept of optical rotation and energy

441   coupling phenomena in the chiral plasmon-exciton systems may have academic significance,

442   opening new doors for chiral bionanosensor development and further studies of chiro-optical

443   memory, chiral catalysis, and light-emitting diodes.

444

Acknowledgements

450

Notes and references

452 1. M. Achermann, *J. Phys. Chem. Lett.,* 2010, **1**, 2837–2843.

453 2. E. Cohen-Hoshen, G. W. Bryant, I. Pinkas, J. Sperling and I. Bar-Joseph, *Nano Lett.,* 2012,

454   **12**, 4260–426.

455 3. J. Lee, P. Hernandez, J. Lee, A. O. Govorov and N. A. Kotov, *Nat. Mater.,* 2007, **6**, 291-295.

456 4. F. Todisco, S. D'Agostino, M. Esposito, A. I. Fernández-Domínguez, M. D. Giorgi,

457   D.Ballarini, L. Dominici, I. Tarantini, M. Cuscuná, F. D. Sala, G. Gigli and D. Sanvitto, *ACS*

458   *Nano,* 2015, **9**, 9691–9699.

459 5. R. Jiang, B. Li, C. Fang and J. Wang, *Adv. Mater.,* 2014, **26**, 5274–5309.

460 6. Q. Zhang, L. Lee, J. B. Joo, F. Zaera, and Y. Yin, *Acc. Chem. Res.,* 2013, **46**, 1816–1824.

461 7. V. K. Valev, J. J. Baumberg, C. Sibilia and T. Verbies, *Adv. Mater.,* 2013, **25**, 2517–2534.

462 8. M. H. Alizadeh and B. M. Reinhard, *ACS Photonics,* 2015, **2**, 942–949.

463 9. Y. Zhao, A. A. E. Saleh and J. A. Dionne, *ACS Photonics,* 2016, **3**, 304–309.

464 10. J. Butet, P. Brevet and O. J. F. Martin, *ACS Nano,* 2015, **9**, 10545–10562.

11. M. Schaferling, X. Yin, N. Engheta and H. Giessen, *ACS Photonics,* 2014, **1**, 530–537.

12. T. Hu, B. P. Isaacoff, J. H. Bahng, C. Hao, Y. Zhou, J. Zhu, X. Li, Z. Wang, S. Liu, C. Xu, J. S. Biteen and N. A. Kotov, *Nano Lett.,* 2014, **14**, 6799–6810.

13. W. Ma, H. Kuang, L. Wang, L. Xu, W. Chang, H. Zhang, M. Sun, Y. Zhu, Y. Zhao, L. Liu, C. Xu, S. Link and N. A. Kotov, *Sci. Rep.,* 2013, **3**, 1934.

14. X. Wu, L. Xu, L. Liu, W. Ma, H. Yin, H. Kuang, L. Wang, C.Xu and N. A. Kotov, *J. Am. Chem. Soc.,* 2013, **135**, 18629–18636.

15. Y. Zhao, L. Xu, W. Ma, L. Wang, H. Kuang, C. Xu and N. A. Kotov, *Nano Lett.,* 2014, **14**, 3908–3913.

16. X. Shen, A. Asenjo-Garcia, Q. Liu, Q. Jiang, F. J. G. D Abajo, N. Liu and B. Ding, *Nano Lett.,* 2013, **13**, 2128–2133.

17. X. Lan, X. Lu, C. Shen, Y. Ke, W. Ni and Q. Wang, *J. Am. Chem. Soc.,* 2015, **137**, 457–462.

18. J. Cheng, G. L. Saux, J.Gao, T. Buffeteau, Y. Battie, P. Barois, V. Ponsinet, M. Delville, O. Ersen, E. Pouget and Reiko Oda, *ACS Nano,* 2017, **11**, 3806–3818.

19. W. Chen, A. Bian, A. Agarwal, L. Liu, H. Shen, L. Wang, C. Xu and N. A. Kotov, *Nano Lett.,* 2009, **9**, 2153–2159.

20. A. J. Mastroianni, S. A. Claridge and A. P. Alivisatos, *J. Am. Chem. Soc.,* 2009, **131**, 8455–8459.

28

483 21. A. Guerrero-Martínez, B. Auguié, J. L. Alonso-Gómez, Z. Džolić, S. Gómez-Graña, M.

484   Žinić, M. M. Cid, L. M. Liz-Marzán, *Angew. Chem.,* 2011, **123**, 5613–5617.

485 22. Z. Fan and A. O. Govorov, *Nano Lett.,* 2010, 10, 2580–2587.

486 23. J. Zho, S.Tang, J. Storhoff, S. Marla, Y. P. Bao, X. Wang, E. Y. Wong, V. Ragupathy,

487   Z. Ye and I. K Hewlett, *BMC Biotechnol.,* 2010, **10**, 74.

488 24. J. Lum, R. Wang, K. Lassiter, B. Srinivasan, D. Abi-Ghanem, L. Berghman, B. Hargis, S.

489   Tung, H. Lu and Y. Li, *Biosens. Bioelectron.,* 2012, **38**, 67–73.

490 25. S. W. Thor, H. Nguyen, A. Balish, A. N. Hoang, K. M. Gustin, P. T.Nhung, J. Jones, N. N.

491   Thu, W. Davis, T. N. T. Ngoc, Y. Jang, K. Sleeman, J. Villanueva, J. Kile, L. V. Gubareva,

492   S. Lindstrom, T. M. Tumpey, C. T. Davis and N. T. Long, *PLOS ONE,* 2015, **10**, e0133867.

493 26. C. Li, D. Cao, Y. Kang, Y. Lin, R. Cui, D. Pang and H. Tang, *Anal. Chem.,* 2016, **88**,

494   4432–4439.

495 27. L. Deng, S. Sharif and É. Nagy, *Clin. Vaccine Immunol.,* 2013, **20**, 1189–1196.

496 28. H. Grgić, D. B. Hunter, P. Hunton and É. Nagy, *Can. J. Vet. Res.,* 2008, **72**, 403–410.

497 29. M. St Paul, N. Barjesteh, J. T. Brisbin, A. Villaneueva, L. R. Read, D. Hodgins, É, Nagy and

498   S. Sharif, *Viral Immunol.* 2014, **27**, 167-173.

499 30. H. S. Alexander, P. Huber, J. Cao, P. J. Krell and E´ Nagy, *J. Virol. Methods,* 1998, **74**, 9–14.

500 31. H. Grgić, D. B. Hunter, P. Hunton and É. Nagy, *Can. J. Vet. Res.,* 2008, **72**, 403–410.

32. J. J. Gelb, 4th ed. The American Association of Avian Pathologists, Dubuque, Iowa: Kendall/Hunt Publ, 1998, 169–175.

33. L. J. Reed and H. Muench, *Am. J. Hyg.* 1938, **27**, 493–497.

34. B. Xiao, S. K. Pradhan, K. C. Santiago, G. N. Rutherford and A. K. Pradhan, *Sci. Rep.,* 2016, **6**, 24385.

35. H. Yockell-Lelievre, F. Lussier and J. Masson, *J. Phys. Chem. C,* 2015, **119,** 28577–28585.

36. Y. Yang, S. Matsubara, M. Nogami, J. Shi and W. Huang, *Nanotechnology,* 2006, **17**, 2821–2827.

37. W. W. Yu, L. Qu, W. Guo and X. Peng, *Chem. Mater.,* 2003, **15**, 2854-2860.